Cardiovascular Research (2013) **100**, 231–240
doi:10.1093/cvr/cvt191

Super-resolution fluorescence microscopy of the cardiac connexome reveals plakophilin-2 inside the connexin43 plaque

Esperanza Agullo-Pascual[1], Dylan A. Reid[2], Sarah Keegan[2,3], Manavjeet Sidhu[1], David Fenyö[2,3]*, Eli Rothenberg[2]*, and Mario Delmar[1]*

[1]The Leon H Charney Division of Cardiology, New York University School of Medicine, 522 First Avenue, Smilow 805, New York, NY 10016, USA; [2]Department of Biochemistry and Molecular Pharmacology, New York University School of Medicine, 522 First Avenue, Smilow 805, New York, NY 10016, USA; and [3]Center for Health Informatics and Bioinformatics, New York University School of Medicine, 227 East 30th Street, Room 739, New York, NY 10016, USA

Received 11 April 2013; revised 26 July 2013; accepted 30 July 2013; online publish-ahead-of-print 8 August 2013

Time for primary review: 40 days

Aims Cell function requires formation of molecular clusters localized to discrete subdomains. The composition of these interactomes, and their spatial organization, cannot be discerned by conventional microscopy given the resolution constraints imposed by the diffraction limit of light (~200–300 nm). Our aims were (i) Implement single-molecule imaging and analysis tools to resolve the nano-scale architecture of cardiac myocytes. (ii) Using these tools, to map two molecules classically defined as components 'of the desmosome' and 'of the gap junction', and defined their spatial organization.

Methods and results We built a set-up on a conventional inverted microscope using commercially available optics. Laser illumination, reducing, and oxygen scavenging conditions were used to manipulate the blinking behaviour of individual fluorescent reporters. Movies of blinking fluorophores were reconstructed to generate subdiffraction images at ~20 nm resolution. With this method, we characterized clusters of connexin43 (Cx43) and of 'the desmosomal protein' plakophilin-2 (PKP2). In about half of Cx43 clusters, we observed overlay of Cx43 and PKP2 at the Cx43 plaque edge. SiRNA-mediated loss of Ankyrin-G expression yielded larger Cx43 clusters, of less regular shape, and larger Cx43-PKP2 subdomains. The Cx43-PKP2 subdomain was validated by a proximity ligation assay (PLA) and by Monte–Carlo simulations indicating an attraction between PKP2 and Cx43.

Conclusions (i) Super-resolution fluorescence microscopy, complemented with Monte–Carlo simulations and PLAs, allows the study of the nanoscale organization of an interactome in cardiomyocytes. (ii) PKP2 and Cx43 share a common hub that permits direct physical interaction. Its relevance to excitability, electrical coupling, and arrhythmogenic right ventricular cardiomyopathy, is discussed.

Keywords Connexin43 • Plakophilin-2 • Ankyrin-G

1. Introduction

Proper cell function requires formation of molecular clusters at discrete subdomains. The composition of these interactomes, and their spatial organization, cannot be discerned by conventional microscopy. In-cell demonstration of physical proximity between two molecules ('co-localization') is hindered by the limited resolution of fluorescence microscopy (~200–300 nm[1]). Antibody-based co-precipitation of molecules fails to determine whether associations are direct or indirect, and involves the loss of cellular compartments. Overall, conventional co-localization or co-precipitation does not resolve whether two molecules are within range of direct interaction (<40 nm). Proximity ligation assays (PLAs) help identify molecular vicinity, but the physical characteristics of the clusters are not defined, given the diffraction limit of light. A recent breakthrough is the development of 'super-resolution' fluorescence microscopy (SRFM) techniques[2] that utilize imaging, chemical, and analytical tools to improve resolution into the range previously reserved for electron microscopy. Recent studies report the use of SRFM in cardiac myocytes to study sarcomeric and dyadic complexes.[3–5] Here, we combine SRFM and Monte–Carlo simulations to characterize the shape, dimensions, physical proximity, and likelihood of co-localization of two proteins of the intercalated disc at a resolution of ~20 nm.

*Corresponding author. Tel: +1 2122639492, Fax: +1 2122634129, Email: mario.delmar@nyumc.org (M.D.)/eli.rothenbreg@nyumc.org (E.R.)/david@fenyolab.org (D.F.)

Our studies focus on two molecules fundamental to intercellular communication: connexin43 (Cx43) and plakophilin-2 (PKP2). PKP2 is classically defined as a desmosomal molecule, necessary for cell–cell adhesion, whereas Cx43 is the primary component of gap junctions. As defined by electron microscopy, desmosomes and gap junctions are distinct electron-dense structures. This has led to the notion that molecules 'of the desmosome' and 'of the gap junction' cannot physically interact. Yet, evidence indicates that molecules of these two complexes can cross-talk.[6–9] Thus, we speculate that though Cx43 and PKP2 populate discrete locations (desmosomes and gap junctions), they also share a common hub that permits direct physical interaction and from which they exert 'non-canonical' functions.[10] The relationship between PKP2 and Cx43 is seen as key in the pathogenesis of arrhythmogenic right ventricular cardiomyopathy (ARVC), an important cause of sudden death in the young.[11]

The formation of functional domains at the membrane is orchestrated, at least in part, by scaffolding molecules that couple the cytoskeleton to integral membrane proteins. A case in point is Ankyrin-G (AnkG), which supports assembly of adhesion points in epithelial cells,[12] and of sodium channel clusters in neurons and heart.[13,14] Recently, we showed that loss of AnkG expression leads to decreased electrical coupling and intercellular adhesion strength in heart cells.[15] This suggests that AnkG participates in formation of a complex involving both electrical and mechanical junctions. Yet, the limited resolution of conventional methods prevented further analysis of such complex.

Here, we implemented SRFM and Monte–Carlo simulations to define, for the first time, the morphology of immuno-reactive Cx43 and PKP2 clusters in intact cells. We demonstrate that the outer edge of Cx43 plaques is also populated by PKP2, and that the dimensions of these clusters depend on AnkG expression. The existence of a Cx43-PKP2 subdomain was confirmed using a PLA both in culture monolayers, and in adult ventricular tissue. We propose that the Cx43-PKP2 subdomain is a shared, interactive hub (a 'connexome') for molecules that control excitability, adhesion, and intercellular communication in the heart.

2. Methods

Neonatal rat ventricular myocytes (NRVMs) were dissociated from hearts of 3–4 day old rats, euthanized by decapitation and removal of the heart, following standard procedures.[9] Conditions for cell culture, western blot, immunofluorescence microscopy, and shRNA-mediated loss of AnkG expression were as in Sato *et al.*[15] PLA protocols were adapted from previous publications[16] and from the manufacturer's instructions. For adult mouse cardiac tissue, we used thin (2–3 μm) sections. Mice were euthanized with an anaesthetic overdose (isoflurane >20%) and confirmed death by cervical dislocation. All the procedures were in accordance with New York University guidelines (IACUC Protocol 101101-02 to MD approved on 7 November 2011) for animal use and care and conformed to the *Guide for the Care and Use of Laboratory Animals* published by the US National Institutes of Health (NIH Publication 58-23, revised 1996).

2.1 SRFM

Super-resolution imaging was done using a custom-built fluorescence microscope (Leica DMI3000) configured for total internal reflection fluorescence (TIRF) and highly inclined excitation modes. The microscopy methods, related calibrations, and controls are detailed in the Supplementary material online, *Figure S1* (see also references[17–22]). Cluster analysis was performed using the ImageJ software, (see also Supplementary material online).

2.2 Monte–Carlo simulations

Simulations were used to define the likelihood and magnitude of signal overlap in an environment where (i) two independent molecular species were randomly and uniformly distributed or (ii) an attraction variable between Cx43 and PKP2 (a 'co-localization factor') was included. Further details are in Supplementary material online.

3. Results

3.1 SRFM

SRFM has been used for nanoscale localization of proteins in subcellular compartments.[3–5,23] Here, we adapted it for the first time to explore the association between intercalated disc molecules. NRVMs were fixed and prepared as for conventional immunofluorescence microscopy. Cx43 and PKP2 were immunolocalized using commercially available antibodies and Alexa fluorophores (A568 and A647 for Cx43 and PKP2, respectively). *Figure 1* shows an image of a site of intercellular contact obtained by conventional TIRF before (*Figure 1A*) and after image reconstruction (*Figure 1B*). Small white squares in (*Figure 1A*) outline areas enlarged in (*Figure 1C*), (*Figure 1D*) and (*Figure 1E*). *Figure 1C* and *D* show diffused diffraction limited resolution of the TIRF image (left), and improved clarity after reconstruction (right). *Figure 1E* shows an enlarged super-resolved image, highlighting physical characteristics consistently observed: a semi-circular Cx43 cluster (green), a neighbouring PKP2 cluster of less defined shape (purple), and an edge of Cx43 where two clusters overlap (white). *Figure 1F* shows a topological image, with signal intensity represented in the *z*-axis. Values of fluorescence amplitude for each protein cluster along a cross-section of the image (dotted line) are plotted in (*Figure 1G*). Note the Gaussian shape of the Cx43 intensity plot, intersected by the PKP2 intensity curve, creating an area of overlap. These overlap areas were seen on the edges of Cx43 plaques, and not in their centre; we did not observe instances, where Cx43 surrounded the PKP2 signal. In contrast to normal distribution of fluorescence intensity across Cx43 clusters, many PKP2 intensity plots were non-Gaussian, displaying long plateaus interrupted by dips, likely reflecting two or more separate clusters, too close to be discerned.

3.2 Physical characteristics of Cx43- and PKP2-immuno-reactive protein clusters in cardiac cells

Super-resolved images (as in *Figure 2A*) were used to measure the area, perimeter, and circularity of clusters, as well as intensity profiles. As shown in *Figure 2B*, the area occupied by individual Cx43 clusters ranged from 8000 to 88 000 nm^2, but the histogram revealed two primary peaks, both defined by Gaussian functions: one with an average value of 13 313 ± 328 nm^2 (± SEM) and the other one at 25 035 ± 227 nm^2. The two peaks were statistically different from one another, with the mean value of the first Gaussian corresponding to near half the mean value of the second Gaussian. Clusters were mostly circular, with a circularity index larger than 0.8 for 65.4% of all clusters examined (*Figure 2C*). As shown in *Figure 2D* and *E*, there was close correlation between area and perimeter of clusters, and between perimeter and circularity, with clusters of smaller dimension being of more circular shape. Clusters with circularity >0.8 were used to characterize fluorescence intensity profiles across the diameter (average plot in *Figure 2F*). Amplitude was normalized to maximum observed in each cluster and distances measured relative to peak of the Gaussian curve. Consistently, Cx43 fluorescence intensity increased

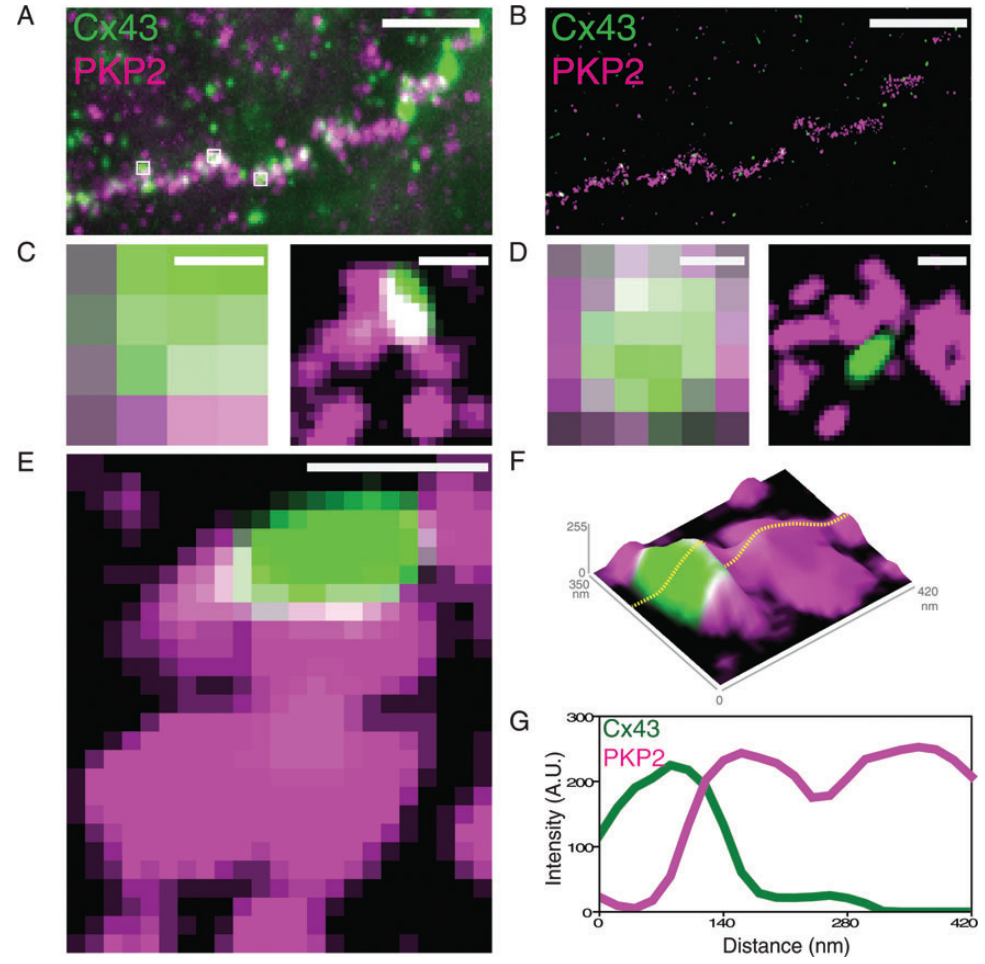

Figure 1 TIRF vs. SRFM. NRVMs stained for Cx43 and PKP2. (*A*) and (*B*) show same region of intercellular contact visualized by TIRF (*A*) and by super-resolution microscopy (*B*). Small white squares in (*A*) are enlarged in (*C*–*E*). (*C*) and (*D*) show improved resolution after reconstruction (right). (*E*) Cx43 cluster surrounded by PKP2, also shown in (*F*) as a topological image (*z*-axis: signal intensity). Dotted line across image is plotted in (*G*) to show intersection of both signals. Scale bars: 5 μm (*A* and *B*) and 200 nm (*C*–*E*).

progressively from periphery to centre, suggesting that Cx43 density is highest in the plaque centre and less towards the periphery, in agreement with freeze-fracture images of gap junction plaques.[24] Results like those described in *Figure 2* were found in cells treated with oligonucleotides that do not affect the expression of relevant proteins (ϕshRNA; see Sato *et al.*[15]; data in Supplementary material online, *Figure S2*). The physical features of Cx43 clusters contrasted with those of PKP2 plaques, which displayed a much broader distribution of area and circularity (Supplementary material online, *Figure S3A–D*), consistent with the idea that PKP2 plaques may be formed by more than one cluster, in very close apposition to each other. Given that limitation, the rest of the quantitative analysis was explored from the perspective of the Cx43 plaques.

3.3 PKP2-immuno-reactive molecules populate the Cx43 cluster: the shared Cx43-PKP2 subdomain

The ability to co-localize fluorescently labelled immuno-reactive proteins with enhanced spatial resolution allowed us to examine proximity of Cx43 to PKP2 (*Figure 3A*). *Figure 3B* displays a histogram of distances separating the edge of Cx43 clusters from the closest edge of a PKP2 plaque. Note that the largest column corresponds to cluster distances of <0, i.e. where the edge of the PKP2 plaque is inside the Cx43 cluster. Overall, 41.9% of Cx43 clusters showed some degree of overlay with PKP2. This result was opposite to the conventional expectation that Cx43 and PKP2 belong to distinct, separate domains of the myocyte. Similar results were observed in cells treated with a non-silencing construct (ϕshRNA; *Figure 3C*). In that case, 57.6% of Cx43 clusters intersected a PKP2 plaque. *Figure 3D* shows a plot correlating area covered by the Cx43-PKP2 subdomain (ordinates), with size of the corresponding Cx43 cluster (abscissa). Black or red circles correspond to clusters measured from untreated (UNT) or ϕshRNA-treated cells, respectively. Identity line (slope of 1) demarcates upper limit of co-localization, i.e. the point at which PKP2 would occupy the entire Cx43 cluster area. The dotted line (slope of 0.5) indicates 50% co-localization. We observed primarily two data groups: the first, contained between the identity line and its 50% reference, showed a relation between Cx43 cluster size and co-localization area (area in light grey). The second one, corresponded to cases where the co-localization area remained $<10\,000$ nm^2 regardless of Cx43 cluster size (light blue). As expected from measurements of Cx43 cluster size (*Figure 2*

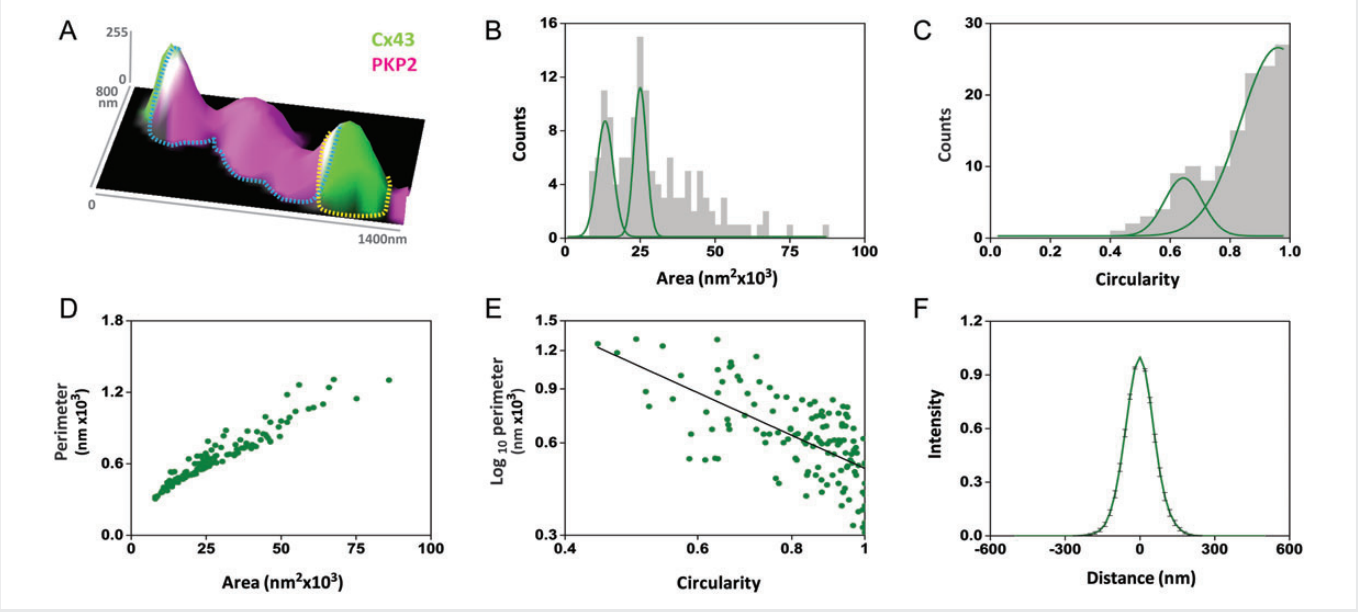

Figure 2 Cx43 cluster analysis. (*A*) Cx43 (green) and PKP2 (purple), with an area of overlap (white). Yellow dotted line demarcates area of Cx43 cluster while blue dotted line demarcates area of PKP2 cluster. (*B*) Histogram of area occupied by each Cx43 cluster. Note two primary Gaussian peaks centred at 13 313 ± 328 and 25 035 ± 226 nm^2. (*C*) Cluster circularity index; a value of 1.0 indicates perfect circle. (*D*) Correlation between area and perimeter. (*E*) Correlation between perimeter and circularity; note that smaller clusters have a more circular shape. (*F*) Average profile of Cx43 fluorescence intensity along the diameter of Cx43 clusters with circularity index >0.8. $n = 136$ clusters of six images analysed.

and Supplementary material online, *Figure S2*), most data points were contained within the 8000 to 60 000 nm^2 range. Next, we assessed whether these parameters depended on AnkG expression.[15] Treatment with a non-silencing construct (ϕshRNA) did not affect the measured parameters and as such, data from UNT and ϕshRNA-treated cells were combined.

3.4 Physical characteristics of the Cx43 clusters depend on AnkG expression

NRVMs were treated with oligonucleotides that prevent AnkG expression (AnkG-shRNA). Western blots confirmed that shRNA treatment prevented AnkG expression (e.g. Supplementary material online, *Figure S4*). *Figure 4A* shows frequency distribution of Cx43 cluster areas in AnkG-silenced cells (red histogram). Gaussian functions describing the control data set are shown as a black line, for comparison (from data in *Figure 2B*). The first Gaussian peak in the AnkG-silenced group, centred at 16 613 ± 322 nm^2, was similar to the first Gaussian peak measured in control (see *Figure 2*). However, a second Gaussian population was not clearly defined. In fact, cluster areas distributed broadly, with areas larger than ~25 000 nm^2. In fact, while 12.3% of the clusters in the control group fell outside the 8000 to 60 000 nm^2 range, there was a larger fraction of clusters > 60 000 nm^2 in the AnkG-silenced group (26.9% of the total). Loss of AnkG expression also correlated with increased number of clusters with a low circularity index (59.9%; *Figure 2B*).

3.5 AnkG expression limits the size of the Cx43-PKP2 subdomain

As shown in Supplementary material online, *Figure S5*, loss of AnkG expression did not reduce the abundance of Cx43 clusters per unit area, but decreased abundance of PKP2 plaques per unit area. Nonetheless, the frequency of Cx43 clusters sharing a subdomain with PKP2 remained similar to control. Indeed, of a total of 381 Cx43 clusters analysed, 54.6% did not show overlap with PKP2 (a proportion similar to that in the control group; see *Figure 3*). On the other hand, the size of the Cx43-PKP2 co-localization area was significantly affected by the absence of AnkG. *Figure 4C* shows the plot correlating area of each Cx43 cluster (abscissa), with that of the corresponding Cx43-PKP2 shared subdomain (ordinates) measured from cells treated with AnkG-shRNA. For reference, the light grey and light blue regions, demarcating areas of this plot occupied by control data, are also depicted. (Same areas as in *Figure 3D*; notice difference in scales.) Clearly, Cx43 clusters in cells lacking AnkG expression showed a wider range of sizes, and the area of co-localization with PKP2 also varied in a wider range. In fact, 40.6% of points in the plot in *Figure 4C* are outside the windows populated by the control data. These results illustrate the power of SRFM to define nano-scale changes in molecular distribution relevant to intercellular communication.

3.6 Monte–Carlo simulations define and quantify the attraction between Cx43 and PKP2

Experimental work was complemented with Monte–Carlo simulations. We first compared the experimentally observed Cx43-PKP2 co-localization, with a model in which clusters of the same size, shape, and density were randomly placed within a similar area of detection. Supplementary material online, *Figure S6–9* compare the physical characteristics of the simulated clusters, with those detected experimentally. *Figure 5A* shows a sample image from the simulations. In contrast to experimental observations (*Figures 3* and *4*), only 20 and 22% of Cx43 clusters simulating control

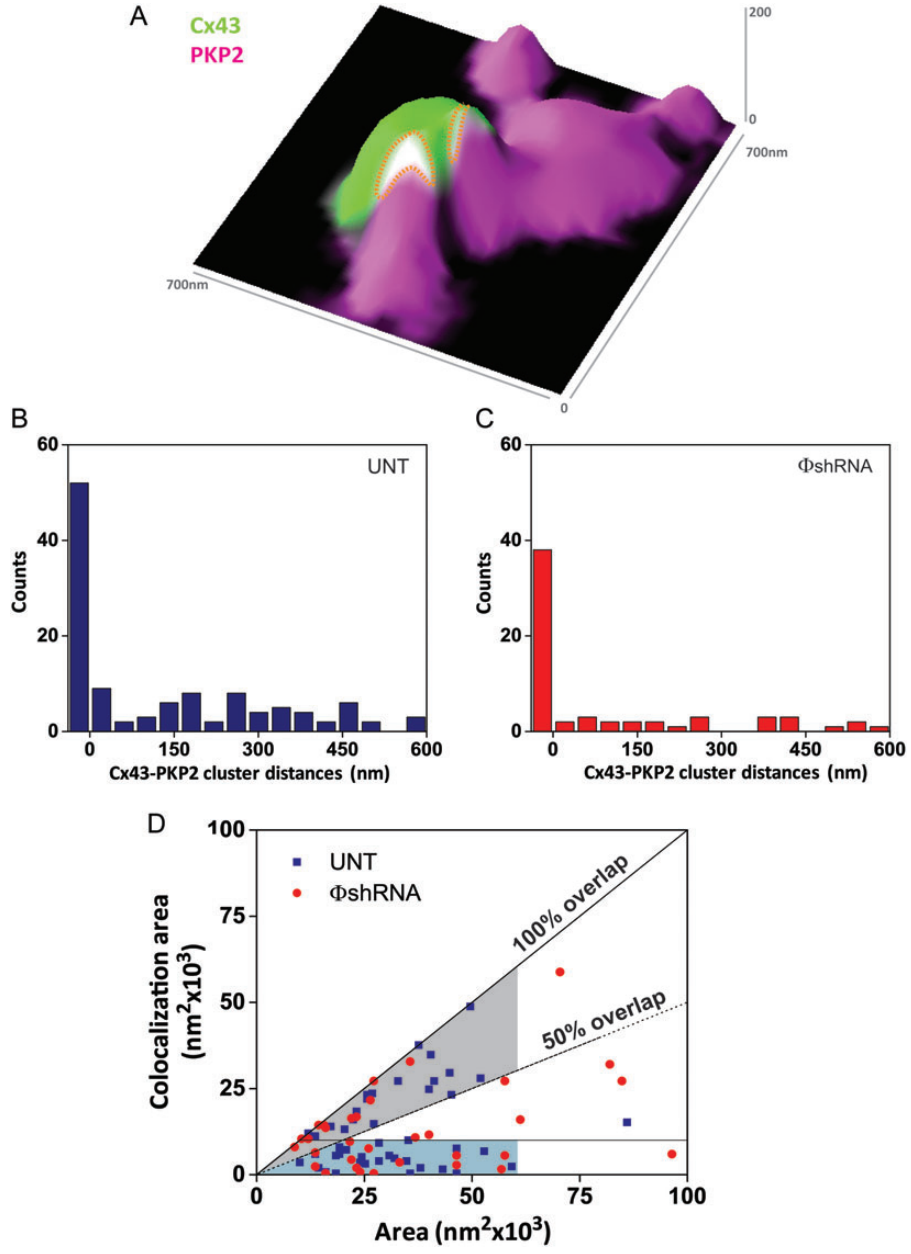

Figure 3 Analysis of Cx43-PKP2 subdomain. (*A*) Example of Cx43 (green) and PKP2 (purple) localization, with an area of overlap (white). Histograms in (*B*) and (*C*) show distances between a Cx43 cluster and the closest PKP2 cluster. (*B*) Untreated cells. (*C*) Cells treated with a control oligonucleotide that does not prevent protein expression. In both histograms, largest number of events (41.9 and 57.6%, respectively), correspond to cases where Cx43 and PKP2 overlap (represented by first bar left of '0 nm' point). (*D*) Scatter plot correlates the Cx43 cluster area with area covered by Cx43-PKP2 subdomain. Grey shade illustrates area between identity line (solid diagonal line) and its 50% reference (dotted diagonal line); blue area highlights clusters with a co-localization of $<10\,000$ nm^2. $n = 124$ and 66, respectively.

and AnkG-silenced cells, respectively, overlapped with a PKP2 cluster. Moreover, the extent of overlap of randomly assigned clusters showed a different profile from that recorded experimentally. Analysis was based on plots of Cx43-PKP2 co-localization as a function of Cx43 cluster area (i.e. *Figures 3D* and *4C*). We separated the data into three groups: points that fell between the identity line and 50% overlap (0.51–1.0), between 10 and 50% overlap (0.1–0.5), and $<$10% overlap ($<$0.1). Experimental data are shown in red and modelled data, in blue. Note the disparity between modelled and experimental results (*Figure 5B*). Although the model predicted a similar probability density along the 0.1–1.0 range, experimental data showed a much higher frequency of events (probability density) for co-localization in the 0.5–1.0 window. These results strongly support the notion of an attraction between Cx43 and PKP2, whereby overlap is not random. Interestingly, the data profile from AnkG-silenced cells suggests that AnkG maintains, at least in part, the attraction between Cx43 and PKP2 (*Figure 5C*).

The simulations above showed that a model based on random distribution did not reproduce experimental data. Complementarily, we

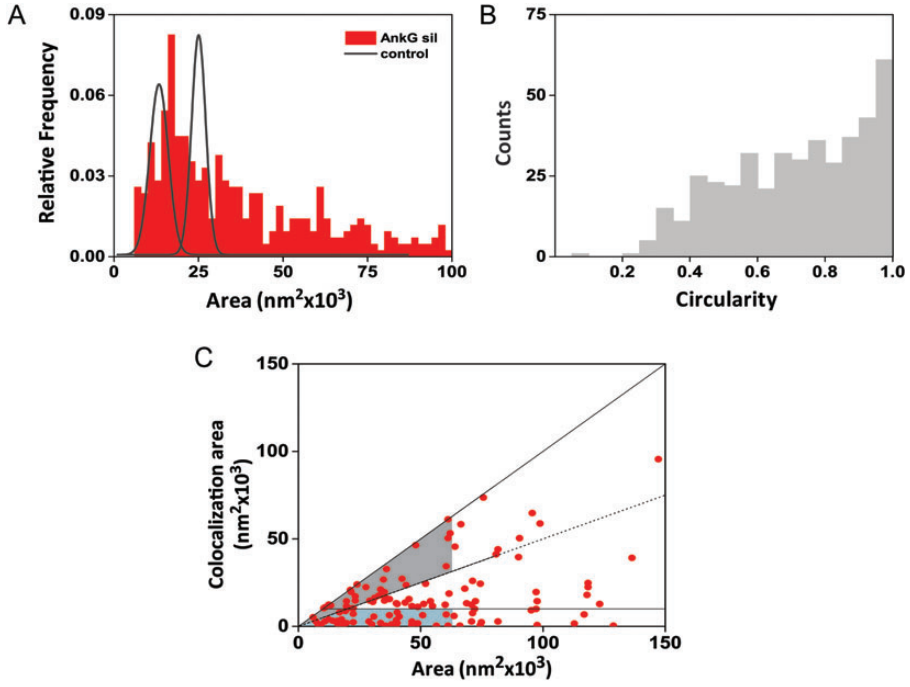

Figure 4 Cx43 cluster dimensions in AnkG-silenced cells. (*A*) distribution of Cx43 cluster areas in AnkG-silenced cells (red histogram) and comparison with Gaussian functions defining Cx43 cluster areas in control (black lines). (*B*) Cluster circularity index in AnkG-silenced cells. $n = 424$ clusters of 12 images analysed. (*C*) Cx43-PKP2 subdomain in cells treated with AnkG-shRNA. Grey and blue areas defined for control cells (*D*) are shown for reference. $n = 128$ clusters.

hypothesized a better experimental-model convergence if Cx43 and PKP2 were treated as mutual attractors (model details in Supplementary material online). *Figures 5D–G* show the probability density for co-localization as a function of a 'co-localization factor', where $f = 1$ was the random condition, and $f = 32$ was the highest co-localization factor tested (further details in Supplementary material online, Methods). *Figure 5D* shows results based on the probability density for co-localization in the 0.5–1.0 range in control conditions, and *Figure 5F*, in the AnkG-silenced cells. Corresponding data for probability density in the 01–0.5 range are shown in *Figure 5E* and *Figure 5G*. In all cases, the green line indicates the value recorded from the experiments (red bars in *Figure 5B* and *C*). Note that the model data progressively approached the experimental value once the co-localization factor was increased and in fact, in the case of AnkG, the plots intersected. These results indicate that Cx43-PKP2 co-localization is not random, and loss of AnkG expression decreases the extent of attraction between the two molecules.

3.7 Cx43 and PKP2 co-localization demonstrated by a PLA

The existence of a shared Cx43-PKP2 space in the intercellular junction interactome was confirmed by PLAs.[16] The tissue was exposed to two antibodies, one recognizing Cx43 and the other one, PKP2, and the two antibodies were ligated and labelled with a single fluorophore. A third antibody was used to detect Cx43 molecules that did not react in the PLA. As shown in *Figure 6A*, we observed abundant Cx43-PKP2 co-localization. The quantification of the number of PLA-positive spots in relation to those only immuno-reactive to the Cx43 antibody is shown in *Figure 6B*. Finally, to prove that the area of Cx43-PKP2 overlap is also a confined subdomain of the adult intercalated disc, we implemented PLAs in sections of mouse cardiac ventricle. As shown in *Figure 6C*, we detected a frequent PLA signal (blue) in the intercalated disc, especially in the direction perpendicular to the long axis of the cells. Cx43 was also detected intermingled with PLA-positive spots. Interestingly, in areas where Cx43 aligned parallel to fibre direction, PLA signals were conspicuously absent, suggesting that Cx43 and PKP2 overlap primarily at the intercalated disc.

4. Discussion

We have used a novel fluorescence microscopy method to localize two cardiac junctional proteins, Cx43, and PKP2, with a spatial resolution previously reserved to the electron microscope. As opposed to EM, where only electron-dense structures can be discerned, SRFM allows for localization of protein clusters using conventional fluorescent-labelled antibodies. A combination of chemical, optical, and analytical manipulations results in identification of the fluorescence source with a spatial resolution that breaks the barrier imposed by the Abbe diffraction limit, estimated at ~250 nm (see van de Linde *et al.*[25] for review on SRFM). In our case, resolution between separate points was ~20 nm, yielding the first co-localization of Cx43 and PKP2-immuno-reactive proteins in cardiac cells at the nanometer scale. We demonstrate that PKP2 and Cx43 are not confined to separate structures but rather, they can overlap in space. The methodological innovation also involved Monte–Carlo simulations to validate and characterize the attraction between PKP2 and Cx43. This is the first study demonstrating the existence of a shared Cx43-PKP2 subdomain within the boundaries of a Cx43 plaque.

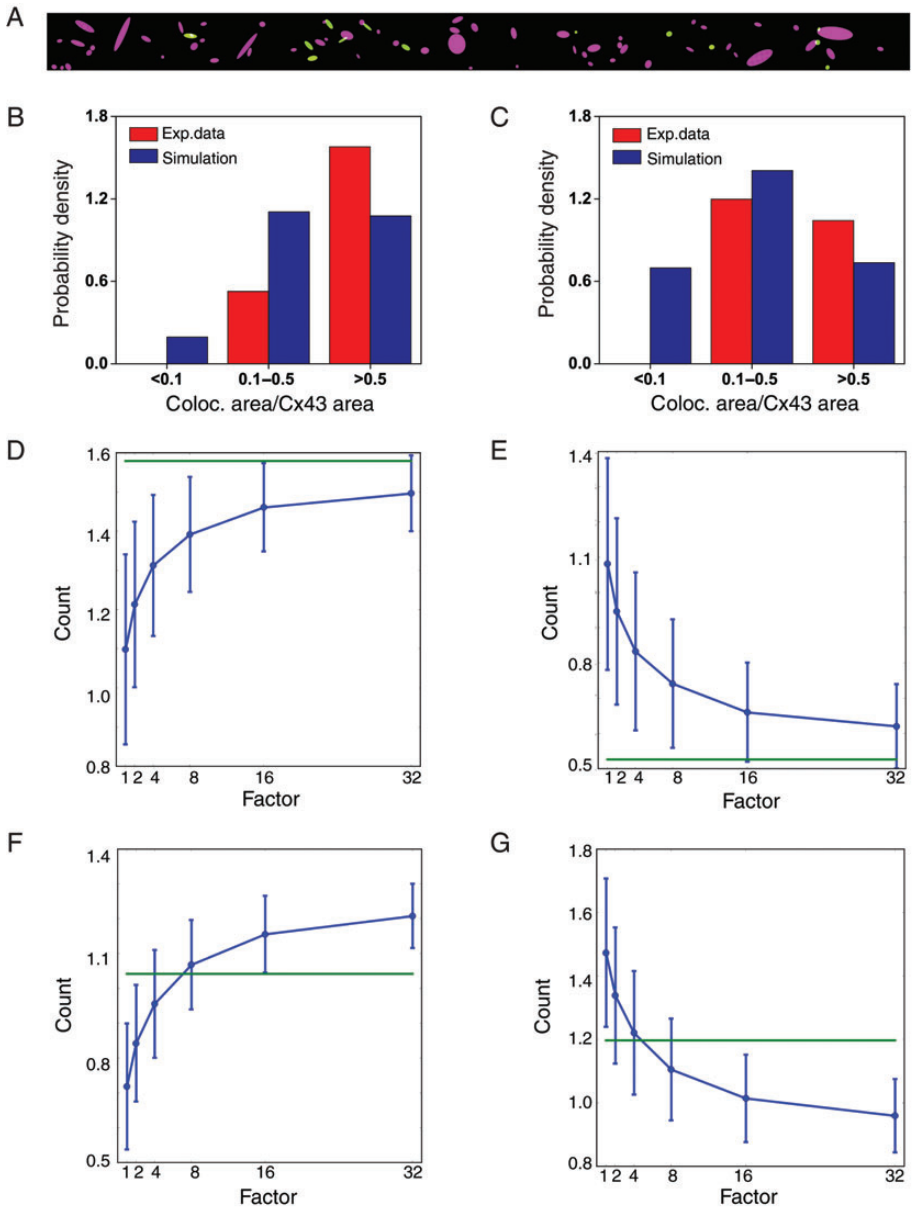

Figure 5 Analysis of the Cx43-PKP2 subdomain by Monte–Carlo simulations. (*A*) Sample image for a simulation of Cx43 and PKP2 clusters drawn as randomly distributed ellipses over a 30 000 × 2000 nm box. (*B*) and (*C*) Correlation Cx43-PKP2 subdomain and Cx43 cluster area of control cells and AnkG-silenced cells, respectively, in experimental data (red) and modelled data (blue). Data are separated in three different groups: >50% overlap, 10–50% overlap or <10% overlap. (*D, E*) and (*F, G*) probability density for co-localization between Cx43 and PKP2 as a function of a 'co-localization factor', i.e. increased Cx43-PKP2 attraction. (*D*) Untreated cells, >50% overlap. (*E*) AnkG-silenced cells, >50% overlap. (*F*) Untreated cells, 10–50% overlap. (*G*) AnkG-silenced cells, 10–50% overlap.

We also show that the dimensions of this domain, and of the entire Cx43 cluster, are restricted by AnkG expression.

4.1 Characteristics of Cx43 clusters

Our data showed that most Cx43 clusters are of two defined dimensions: one of ~25 000 nm^2 and the other one of approximately half that size. A third group corresponded to larger clusters, though not larger than ~ 90 000 nm^2. In the Cx43 life cycle, at least three types of Cx43 aggregates can be found at or near the membrane: a connexon, a gap junction, and the 'connexosomes', representing large Cx43-rich membrane vesicles. We speculate that the three sizes correspond to each of those stages. Interestingly, loss of AnkG, known to decrease junctional conductance,[15] associated with decreased amplitude of the second Gaussian peak. Additional experiments will be needed to confirm the relationship between cluster size and functional state.

4.2 Interaction of Cx43 with PKP2 and with AnkG

As stated in Supplementary material online, Methods, we calculated the final axial imaging volume after rejection in our set-up to be ≤160 nm. In the *X–Y* plane, when considering only Cx43 clusters within the two

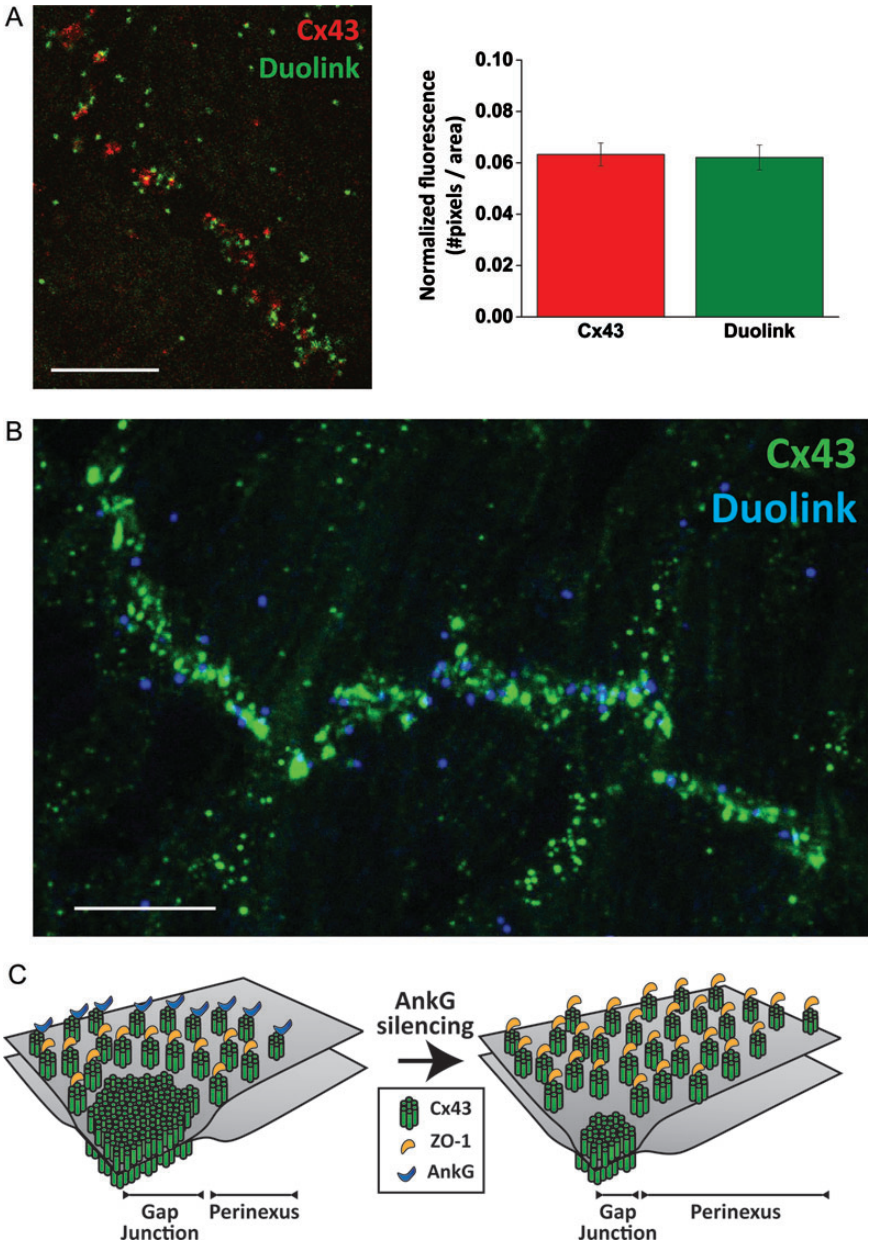

Figure 6 (*A*) Cx43-PKP2 interaction in rat heart tissue, detected by a proximity ligation assay (Duolink). Cx43-PKP2 cross-reactivity by PLA is shown in blue. Cx43 alone is depicted in green. Scale bar = 10 μm. (*B*) Proposed model of Cx43 plaque organization. The gap junction is surrounded by an area defined as the perinexus where Cx43 hemichannels interact with ZO-1; this interaction regulates the transition of connexons to the gap junction.[16] We speculate that AnkG is localized at the border of the perinexus; we further speculate that AnkG and ZO-1 are mutually exclusive and in this manner, AnkG restricts plaque size. When AnkG is silenced (right panel), the area of influence of ZO-1 increases, expanding the perinexal area at the expense of the actual pore-forming gap junction, yielding larger Cx43 plaque sizes and yet, a reduced channel-forming domain.

Gaussians in *Figure 2B*, average cluster diameter was ~150 nm. The circular *X*–*Y* projections originated from three-dimensional gap junction plaques, likely raising several tenths of nanometers in the *z*-plane. Similarly, PKP2 plaques occupied a large area (see Supplementary material online, *Figure S3*) and likely represent a volume where clusters raise several tenths of nanometers on the *z*-plane. We show overlap of Cx43 and PKP2 signals. That is, at least part of Cx43 and PKP2 clusters occupy the same axial imaging volume. Considering the size of each individual cluster, and our knowledge on the dimensions of gap junction and desmosome plaques, it is unlikely that our results are consequent to the presence of a desmosome standing on top of a gap junction, both fitting within the axial imaging volume after rejection without reaching an interactive range. Rather, our results argue in favour of the idea that PKP2 is present within the confines of a Cx43 plaque.

We demonstrated that the spatial domain of a Cx43 plaque often includes PKP2 molecules. This is consistent with data showing PKP2 and Cx43 in the same precipitate. Yet, we also showed that a fraction of Cx43 plaques did not contact PKP2. We speculate that the Cx43-PKP2 association occurs only within a given window of the Cx43 plaque life cycle. The characteristics of such association are not

known. What is clear is that PKP2 expression and/or structural integrity is necessary to preserve gap junctions.[6]

AnkG is a cytoskeletal adaptor protein. In the heart, as in other structures such as the nodes of Ranvier,[26] AnkG couples the pore-forming alpha subunit of the sodium channel to the actin cytoskeleton.[13] In cardiac myocytes, AnkG co-precipitates and functionally interacts with Cx43.[15] Here, we show that loss of AnkG expression allowed formation of large Cx43 plaques. This is reminiscent of the observation in myelinated axons, where Na_V-associated scaffolding proteins act as barriers to restrict invasion of flanking paranodal domains.[27] We propose that AnkG flanks and restricts Cx43 cluster size. Interestingly, loss of AnkG expression leads to decreased electrical coupling between cells.[15] This inverse relationship between Cx43 plaque size and Cx43-mediated electrical coupling supports the notion that only a fraction of Cx43 forms functional gap junctions, and such a fraction can be regulated independently from factors that control plaque size.

4.3 Defining Cx43 subdomains: the perinexus and the 'connexome'

Regulation of Cx43 plaque size has been extensively studied for zonula occludens-1 (ZO-1). Recent studies showed that Cx43-ZO-1 association occurs in the periphery of the Cx43 plaque (the 'perinexus')[16] and that loss of ZO-1 interaction leads to larger gap junction plaques, with loss of perinexus space. Here, we report that loss of AnkG caused increased abundance of plaques of larger size. Yet, this manipulation also caused reduced electrical coupling.[15] We speculate that AnkG and ZO-1 are mutually exclusive, so that the perinexal space is restricted by the presence of AnkG at its border (*Figure 6D*). Accordingly, loss of AnkG would allow expansion of the perinexus, increasing Cx43-ZO-1 contact area and thus, further limiting access of Cx43 to the inner core of the plaque, where gap junctions are formed (*Figure 6D*, right panel).

The functional consequences of associations in the perinexus likely extend beyond formation of electrical or mechanical junctions. Recent studies show non-canonical, gap junction-independent functions of Cx43.[10] Key among them is preservation of sodium current amplitude.[28,29] In fact, mutations in Cx43 can cause ventricular arrhythmias and sudden death even when electrical coupling is preserved.[30] PKP2 also regulates amplitude and gating behaviour of the sodium current.[9] The observation that both $Na_V1.5$[31] and PKP2 are in physical contact with Cx43 leads us to suggest that the Cx43 plaque hosts a molecular complex (a 'connexome') that regulates electrical coupling, cell adhesion, and cell excitability.

4.4 The connexome and ARVC pathogenesis

The existence of PKP2 as part of the connexome is contrary to the perception of PKP2 as a component of mechanical junctions that only interact with Cx43 in a distant, and indirect manner. The possibility of direct Cx43-PKP2 cross-talk is relevant to the molecular pathophysiology of ARVC (or AC; see Delmar and McKenna[32]). Mutations in PKP2 are the most common cause of familial ARVC. Loss of Cx43 plaques is a common finding in ARVC-affected hearts[11] and in cells lacking PKP2.[6] The mechanism by which a 'desmosomal molecule' such as PKP2 leads to loss of Cx43 plaques has puzzled investigators. Our data show that the cause of PKP2-dependent loss of Cx43 plaques does not need to be indirect. These molecules are likely direct partners, co-inhabitants of a physical space, and the structural integrity of one is likely to be necessary for the preservation of the other and of the connexome as a whole. Our results provide a novel angle to better understand the relationship between sequence integrity of PKP2, and occurrence of deadly arrhythmias in young patients, even in the absence of overt structural disease.[32]

Supplementary material

Supplementary material is available at *Cardiovascular Research* online.

Conflict of interest: none declared.

Funding

Supported by grants from National Institutes of Health (R01-HL106632 and R01-GM57691 to M.D, and U54-RR02220 to D.F.), and Leducq Foundation Transatlantic Network (M.D).

References

1. Born MW, E. *Principles of Optics: Electromagnetic Theory of Propagation, Interference and Diffraction of Light*. Cambridge: Cambridge University Press, 1997.
2. Heilemann M, van de Linde S, Schuttpelz M, Kasper R, Seefeldt B, Mukherjee A *et al*. Subdiffraction-resolution fluorescence imaging with conventional fluorescent probes. *Angew Chem Int Ed Engl* 2008;**47**:6172–6176.
3. Baddeley D, Jayasinghe ID, Lam L, Rossberger S, Cannell MB, Soeller C. Optical single-channel resolution imaging of the ryanodine receptor distribution in rat cardiac myocytes. *Proc Natl Acad Sci U S A* 2009;**106**:22275–22280.
4. Soeller C, Baddeley D. Super-resolution imaging of EC coupling protein distribution in the heart. *J Mol Cell Cardiol* 2013;**58**:32–40.
5. Wong J, Baddeley D, Bushong EA, Yu Z, Ellisman MH, Hoshijima M *et al*. Nanoscale distribution of ryanodine receptors and caveolin-3 in mouse ventricular myocytes: dilation of T-tubules near junctions. *Biophys J* 2013;**104**:L22–L24.
6. Oxford EM, Musa H, Maass K, Coombs W, Taffet SM, Delmar M. Connexin43 remodeling caused by inhibition of plakophilin-2 expression in cardiac cells. *Circ Res* 2007;**101**:703–711.
7. Asimaki A, Tandri H, Huang H, Halushka MK, Gautam S, Basso C *et al*. A new diagnostic test for arrhythmogenic right ventricular cardiomyopathy. *N Engl J Med* 2009;**360**:1075–1084.
8. Li J, Patel VV, Kostetskii I, Xiong Y, Chu AF, Jacobson JT *et al*. Cardiac-specific loss of N-cadherin leads to alteration in connexins with conduction slowing and arrhythmogenesis. *Circ Res* 2005;**97**:474–481.
9. Sato PY, Musa H, Coombs W, Guerrero-Serna G, Patino GA, Taffet SM *et al*. Loss of plakophilin-2 expression leads to decreased sodium current and slower conduction velocity in cultured cardiac myocytes. *Circ Res* 2009;**105**:523–526.
10. Agullo-Pascual E, Delmar M. The noncanonical functions of Cx43 in the heart. *J Membr Biol* 2012;**245**:477–482.
11. Kaplan SR, Gard JJ, Protonotarios N, Tsatsopoulou A, Spiliopoulou C, Anastasakis A *et al*. Remodeling of myocyte gap junctions in arrhythmogenic right ventricular cardiomyopathy due to a deletion in plakoglobin (Naxos disease). *Heart Rhythm* 2004;**1**:3–11.
12. Kizhatil K, Davis JQ, Davis L, Hoffman J, Hogan BL, Bennett V. Ankyrin-G is a molecular partner of E-cadherin in epithelial cells and early embryos. *J Biol Chem* 2007;**282**:26552–26561.
13. Lowe JS, Palygin O, Bhasin N, Hund TJ, Boyden PA, Shibata E *et al*. Voltage-gated Nav channel targeting in the heart requires an ankyrin-G dependent cellular pathway. *J Cell Biol* 2008;**180**:173–186.
14. Zhou D, Lambert S, Malen PL, Carpenter S, Boland LM, Bennett V. Ankyring is required for clustering of voltage-gated Na channels at axon initial segments and for normal action potential firing. *J Cell Biol* 1998;**143**:1295–1304.
15. Sato PY, Coombs W, Lin X, Nekrasova O, Green KJ, Isom LL *et al*. Interactions between ankyrin-G, Plakophilin-2, and Connexin43 at the cardiac intercalated disc. *Circ Res* 2011;**109**:193–201.
16. Rhett JM, Jourdan J, Gourdie RG. Connexin 43 connexon to gap junction transition is regulated by zonula occludens-1. *Mol Biol Cell* 2011;**22**:1516–1528.
17. Henriques R, Lelek M, Fornasiero EF, Valtorta F, Zimmer C, Mhlanga MM. QuickPALM: 3D real-time photoactivation nanoscopy image processing in ImageJ. *Nat Methods* 2010;**7**:339–340.
18. Malkusch S, Muranyi W, Muller B, Krausslich HG, Heilemann M. Single-molecule coordinate-based analysis of the morphology of HIV-1 assembly sites with near-molecular spatial resolution. *Histochem Cell Biol* 2013;**139**:173–179.
19. Yamaguchi S, Reid DA, Rothenberg E, Darwin AJ. Changes in Psp protein binding partners, localization and behaviour upon activation of the Yersinia enterocolitica phage shock protein response. *Mol Microbiol* 2013;**87**:656–671.

20. Hong M, Bao L, Kefaloyianni E, Agullo-Pascual E, Chkourko H, Foster M *et al*. Heterogeneity of ATP-sensitive K+ channels in cardiac myocytes: enrichment at the intercalated disk. *J Biol Chem* 2012;**287**:41258–41267.
21. Chkourko HS, Guerrero-Serna G, Lin X, Darwish N, Pohlmann JR, Cook KE *et al*. Remodeling of mechanical junctions and of microtubule-associated proteins accompany cardiac connexin43 lateralization. *Heart Rhythm* 2012;**9**:1133–1140 e1136.
22. Simonson PD, Rothenberg E, Selvin PR. Single-molecule-based super-resolution images in the presence of multiple fluorophores. *Nano Lett* 2011;**11**:5090–5096.
23. Dani A, Huang B, Bergan J, Dulac C, Zhuang X. Superresolution imaging of chemical synapses in the brain. *Neuron* 2010;**68**:843–856.
24. Palatinus JA, Rhett JM, Gourdie RG. The connexin43 carboxyl terminus and cardiac gap junction organization. *Biochim Biophys Acta* 2012;**1818**:1831–1843.
25. van de Linde S, Loschberger A, Klein T, Heidbreder M, Wolter S, Heilemann M *et al*. Direct stochastic optical reconstruction microscopy with standard fluorescent probes. *Nat Protoc* 2011;**6**:991–1009.
26. Kordeli E, Lambert S, Bennett V, Ankyrin G. A new ankyrin gene with neural-specific isoforms localized at the axonal initial segment and node of Ranvier. *J Biol Chem* 1995;**270**:2352–2359.
27. Thaxton C, Pillai AM, Pribisko AL, Dupree JL, Bhat MA. Nodes of Ranvier act as barriers to restrict invasion of flanking paranodal domains in myelinated axons. *Neuron* 2011;**69**:244–257.
28. Jansen JA, Noorman M, Musa H, Stein M, de Jong S, van der Nagel R *et al*. Reduced heterogeneous expression of Cx43 results in decreased Nav1.5 expression and reduced sodium current that accounts for arrhythmia vulnerability in conditional Cx43 knockout mice. *Heart Rhythm* 2012;**9**:600–607.
29. Desplantez T, McCain ML, Beauchamp P, Rigoli G, Rothen-Rutishauser B, Parker KK *et al*. Connexin43 ablation in foetal atrial myocytes decreases electrical coupling, partner connexins, and sodium current. *Cardiovasc Res* 2012;**94**:58–65.
30. Lubkemeier I, Requardt RP, Lin X, Sasse P, Andrie R, Schrickel JW *et al*. Deletion of the last five C-terminal amino acid residues of connexin43 leads to lethal ventricular arrhythmias in mice without affecting coupling via gap junction channels. *Basic Res Cardiol* 2013;**108**:348.
31. Rhett JM, Ongstad EL, Jourdan J, Gourdie RG. Cx43 associates with Na(v)1.5 in the cardiomyocyte perinexus. *J Membr Biol* 2012;**245**:411–422.
32. Delmar M, McKenna WJ. The cardiac desmosome and arrhythmogenic cardiomyopathies: from gene to disease. *Circ Res* 2010;**107**:700–714.